ELSEVIER

Nuclear Instruments and Methods in Physics Research A 484 (2002) 396–406

NUCLEAR INSTRUMENTS & METHODS IN PHYSICS RESEARCH Section A

www.elsevier.com/locate/nima

Evaluation of a photon-counting hybrid pixel detector array with a synchrotron X-ray source

C. Ponchut[a,*], J.L. Visschers[b], A. Fornaini[b], H. Graafsma[a], M. Maiorino[c], G. Mettivier[c], D. Calvet[b,d]

[a] *European Synchrotron Radiation Facility (ESRF), 6 rue Jules Horowitz, BP 220, F-38043 Grenoble, France*

[b] *National Institute for Nuclear Physics and High Energy Physics (NIKHEF), P.O. Box 41882, NL 1009 DB Amsterdam, Netherlands*

[c] *Dipartimento di Scienze Fisiche, Università di Napoli "Federico II" and INFN, Via Cintia, 80126 Napoli, Italy*

[d] *Centre de Physique des Particules de Marseille (CPPM), 163 Avenue de Luminy, Case 907, 13288 Marseille cedex 9, France*

Received 12 June 2001; received in revised form 4 September 2001; accepted 10 September 2001

Abstract

A photon-counting hybrid pixel detector (Medipix-1) has been characterized using a synchrotron X-ray source. The detector consists of a readout ASIC with 64×64 independent photon-counting cells of $170 \times 170\,\mu m^2$ pitch, bump-bonded to a 300 μm thick silicon sensor, read out by a PCIbus-based electronics, and a graphical user interface (GUI) software. The intensity and the energy tunability of the X-ray source allow characterization of the detector in the time, space, and energy domains. The system can be read out on external trigger at a frame rate of 100 Hz with 3 ms exposure time per frame. The detector response is tested up to more than 7×10^5 detected events/pixel/s. The point-spread response shows $<2\%$ crosstalk between neighboring pixels. Fine scanning of the detector surface with a 10 μm beam reveals no loss in sensitivity between adjacent pixels as could result from charge sharing in the silicon sensor. Photons down to 6 keV can be detected after equalization of the thresholds of individual pixels. The obtained results demonstrate the advantages of photon-counting hybrid pixel detectors and particularly of the Medipix-1 chip for a wide range of X-ray imaging applications, including those using synchrotron X-ray beams.

PACS: 29.40.Wk; 42.59.Pw; 87.59.e

Keywords: Hybrid pixel detector; Medipix; X-ray imaging; Synchrotron; Photon-counting

1. Introduction

The Medipix-1 circuit [1] is a photon-counting readout circuit developed in the framework of the MEDIPIX collaboration, based at CERN (see also: http://www.cern.ch/MEDIPIX/). When bump-bonded to a matrix of semiconducting sensor diodes, such circuits form hybrid X-ray detectors of interest for medical and biological imaging applications. Their advantages are high sensitivity, linearity, uniformity and dynamic range.

Medipix-1 has already undergone several evaluations demonstrating its imaging capabilities [2–6] using conventional X-ray sources. In order to

*Corresponding author. Tel.: +33-0476-88-2117; fax: +33-0476-88-2542.

E-mail address: ponchut@esrf.fr (C. Ponchut).

0168-9002/01/$ - see front matter
PII: S0168-9002(01)02029-0

extend the circuit evaluation towards the high flux regime and thus demonstrate its potential use for a wider range of applications, an evaluation using an intense synchrotron X-ray source was carried out, allowing to reach count rates of more than 1 MHz/pixel corresponding to flux rates of more than 3.4×10^7 monochromatic photons/mm^2/s which is not reachable with a conventional X-ray source. This paper reports results in particular on: energy response, linearity at high count rates, spatial response at the sub pixel scale related to charge sharing effects, and time resolution capabilities.

2. System description

2.1. Detector assembly

Medipix is an integrated circuit, designed in SACMOS 1 μm technology, consisting of 4096 individual pixels arranged in a 64×64 matrix. Each pixel contains a low-noise amplifier, a pulse shaper, an individually tunable threshold comparator and a 15-bit counter [1,7]. The circuit is bump-bonded to a sensor chip with a corresponding matrix of 64×64 reverse biased detector diodes, surrounded by a single guard ring structure. Such hybrid sandwiches are excellent X-ray imaging devices for energy ranges that depend on the material chosen for the sensor chip (silicon, gallium arsenide or cadmium zinc telluride). In our case, the sensor chip material is high purity silicon with a resistivity of 10 kΩ cm and a thickness of around 300 μm. The sensor is operated in full depletion with a reverse bias of 100 V. The Medipix detector assembly is glued with conductive glue on a small printed circuit board that directly connects to a metal box, containing the MUROS-1 [8] acquisition electronics. Wire bonding is used to connect the CMOS chip to the gold-plated pads on this board.

2.2. Acquisition system

The Medipix-1 chip is read out via commercially available analog and digital I/O cards. Connection between such cards and the detector chip is made via a Medipix-1 re-Usable Read-Out System (MUROS-1), a small electronics box translating the TTL levels of the PCIbus cards to the CMOS levels needed by Medipix-1, and vice versa. Also included on the MUROS-1 board is a test-pulse generating circuit, and a provision to tune the reverse bias voltage. Both these options can also be controlled via the same PCIbus cards. Commercial cards used are the National Instruments (NI) AT-AO 10[1] for the analog voltage supplies and the chip control lines, and the PCI-DIO 32HS[1] for the bi-directional digital data bus and the clock. These cards are plugged into a standard 550 MHz 128 Mb Pentium-III®[2] Personal Computer (PC), running the LabWindows/CVI®[1] programming environment under Windows NT.[3]

The AT-AO 10 card has ten analog output lines among which seven are used, five for the analog voltages (biases, thresholds, etc.) and two for generating the test pulse. Five out of the eight digital I/O lines from this card are also used to control the detector (shutter, reading/writing, chip select, data/control and reset). Power supply for MUROS-1 and for the Medipix-1 chip is drawn directly from the PC via this card.

The PCI-DIO 32HS card has 32 digital I/O lines, among which 16 are used for data communication. Eight more lines are available for clocking purposes, but only one is used to synchronize chip and PC. The card communicates with the Medipix-1 chip at a maximum rate of 20 Mbytes/s.

The system is robust and portable, and needs no separate power supplies, pulse generators or bulky instrumentation crates.

2.3. Acquisition software

Medisoft (version 3.1) is a software package written in ANSI C under LabWindows/CVI development environment that makes extensive

[1] The AT-AO-10, PCI-DIO-32HS and PCI-1200 boards and the LabWindows/CVI software are products of National Instruments Corporation, 6504 Bridge Point Parkway, Austin, TX 78730-5039, USA.

[2] Pentium-III is a product of INTEL Corporation, 2200 Mission College Blvd., Santa Clara, CA 95052-8119, USA.

[3] Windows NT is a product of Microsoft Corporation, One Microsoft Way, Redmond, WA 98052-6399, USA.

use of the LabWindows data acquisition libraries and GUI capabilities. It automatically detects the fastest communication speed between PC and Medipix, independent of the specific hardware configuration. Algorithms are available for equalizing the comparator settings of the individual pixels thus, equalizing the threshold values of every single pixel to improve the detector uniformity. With this package, it is possible to acquire and display images and to perform spectroscopic measurements by acquiring sequences of images taken at increasing detection thresholds. In order to implement acquisition features of interest for the present study, some powerful features have been implemented (Medisoft v. 3.1.1). They include the high frame rate acquisition (100 Hz, 30% duty cycle) driven by an external trigger signal, high-statistics spectra acquisition and "movie grabbing" (up to 500 frames).

3. Experimental setup

The detector was installed in the multipurpose station of the BM5 ESRF beam line which can deliver a monochromatic beam in the 4–30 keV range with an intensity of 10^9 X-ray photons/s (Fig. 1). Two sets of double collimators control the beam cross-section which can be set as small as $10 \times 10\,\mu m^2$. The beam intensity is monitored using a large-area silicon photodiode with 300 μm thickness. The detector assembly is fixed perpendicular to the beam axis on a translation stage with axial, lateral, and vertical motion, allowing submicron positioning in both lateral and vertical directions as well as axial rotation. The distance from the last collimator to the detector is approximately 50 cm. For most tests, the beam energy was set to 13 keV, which is close to the energies most often used at the ESRF for soft matter analysis by X-ray diffraction or X-ray scattering. At this energy, the absorption efficiency of the 300 μm silicon sensor is 60%, hence 40% of the photons are undetected and hit the readout circuit.

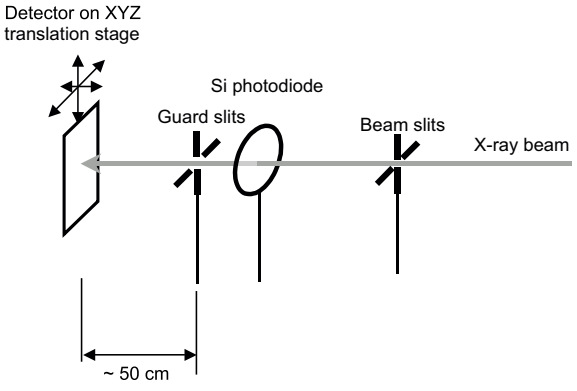

Fig. 1. Experimental setup.

4. Imaging tests

4.1. Spatial uniformity, threshold equalization

To test the uniformity, a large spot size is needed. Due to the special properties of a synchrotron beam, and because of special limitations in the BM5 beam line, the largest beam size obtainable was $6 \times 3\,mm^2$. Intensity in this wide beam was not completely uniform but shows part of an elliptical intensity distribution.

Fig. 2a shows the result of a 10 s exposure with a beam of 13 keV and all pixel threshold voltages set to the same value ($V_{th} = 1.0$ V). The rectangular collimator is clearly visible, but the uniformity is poor. The pixel count distribution shows a significant amount of exposed pixels (about 5%) with less than 50% of the mean count (Fig. 2b). Furthermore, the unexposed region contains many noisy pixels. These problems are caused by differences in the transistor characteristics for different pixels. The CMOS process used (SACMOS-1) is normally used for digital circuits and the matching between transistors is not optimal, resulting in large amplifier gain variations between different pixels. Therefore, the designers of this chip [1,7] included in every pixel a 3-bits Digital to Analog Converter (DAC), adjustable via software, to correct for this effect. The range of these DAC's is controlled by a common threshold adjust voltage $V_{tha.}$ A threshold adjustment procedure is presented in Ref. [9].

Fig. 2c shows the result for the same exposure but now with $V_{th} = 0.9$ V, $V_{tha} = 0.55$ V, and every

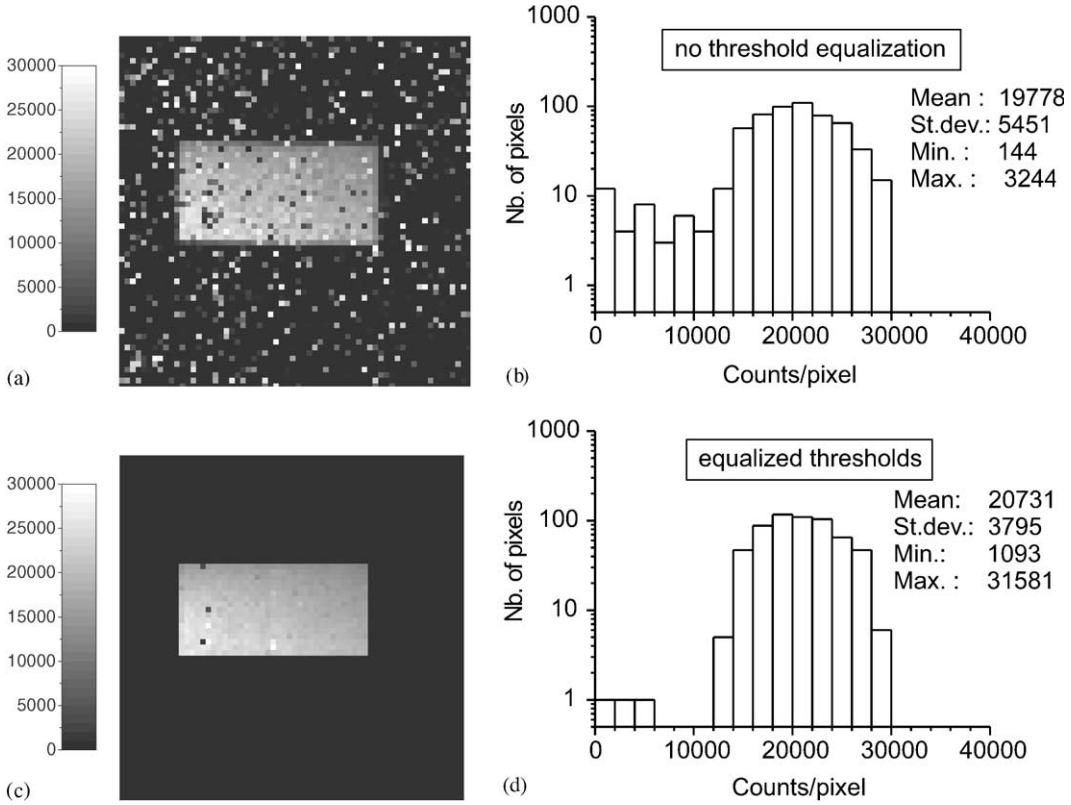

Fig. 2. Image of a large rectangular X-ray beam and histogram of the pixel counts in the exposed region, without threshold equalization (a and b), and with threshold equalization (c and d). Both histograms refer to the same exposed detector area of $35 \times 17 = 595$ pixels.

individual DAC set to its optimal 3-bit value. The noisy pixels outside the beam area have been masked; those inside reduced. The uniformity has improved a lot, the population of low count pixels is suppressed with exception of 3 defective pixels (Fig. 2d).

4.2. Energy calibration, ENC

To obtain the energy calibration of our detector, different X-ray energies are needed. Thus, we used beam energies of 6, 8, 13, 15, 18 and 21 keV. The accuracy on these values is 1%. For each given energy, we performed a threshold scan over an area of 10×10 pixels hit by the beam: in such a scan, the threshold voltage setting in mV is scanned from 800 to 1400 mV, in steps of 10 mV. For each value, we make an image acquisition, and obtain the count rate as a function of threshold voltage (S-curve). All this procedure can be automatically managed via software. For every pixel, we have six curves, corresponding to the six different energies employed. The number of counted photons is about 10^4 per pixel at low thresholds, decreasing to almost zero around the upper limit of our scan. At higher energies, the count rate is further reduced because 300 μm of silicon do not fully absorb the X-rays: for instance at a beam energy of 21 keV only 22% of the photons are stopped. Some bad pixels were excluded from the analysis, leaving us with a total of 88 good pixels to analyze.

The S-curves are first differentiated: the resulting peaked distributions can be fitted with

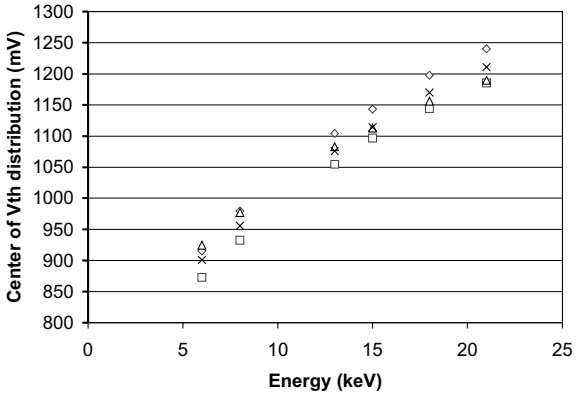

Fig. 3. Absolute energy calibration for 4 arbitrary pixels.

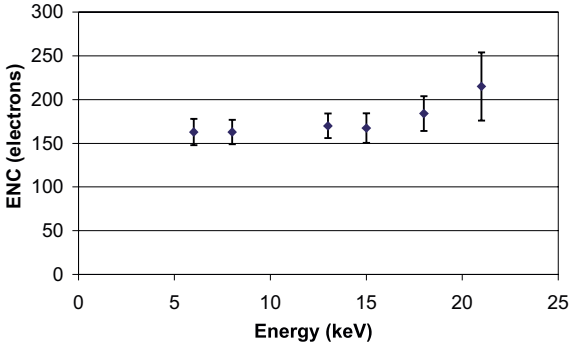

Fig. 4. ENC as function of X-ray energy, averaged over 88 pixels. The error bars indicate the spread over the pixels.

Gaussian functions, giving two useful quantities for our analysis: the center of the differentiated distribution μ_{mV} and the Gaussian spread σ_{mV}, both in mV. We have six values of μ_{mV} and six values of σ_{mV} for every analyzed pixel, corresponding to the six beam energies.

The μ_{mV} contain the energy calibration. For every pixel, the voltage thresholds μ_{mV} were plotted as a function of the beam energy (in keV) and then a quadratic fit gave us the needed calibration function. In this way, we obtained 88 calibration functions, one for each pixel. Four arbitrary ones are shown in Fig. 3.

The σ_{mV} contain information on the Equivalent Noise Charge (ENC), measured as equivalent electron charges on the amplifier input. Using our calibration functions we translate the σ_{mV} from mV to keV, and then from keV to electrons just by multiplying by 1000 and dividing by k, where

$$k = 3.62\,\mathrm{eV/e^-}$$

is the energy needed to create an electron/hole pair in silicon. For each of the six different energies we now have 88 ENC values σ_{ENC}, one for each pixel.

For each energy, we studied the distribution of the so-obtained ENC value over the 88 pixels, fitting these distributions again with a Gaussian function: in Fig. 4, the mean of this distribution is shown as a function of beam energy, while its standard deviation is taken as an error bar.

The result of 163 electrons (ENC) at an X-ray energy of 8 keV is to be compared with our previously reported result of 142 electrons [4], obtained with a different Medipix silicon assembly and using only two X-ray energies with linear fits for the calibration functions. The average noise over the investigated energy range is estimated to be 170 electrons.

4.3. Linearity

An effort was made to determine the linearity of the response as a function of pixel input rate. Different beam intensities were created with aluminum attenuator foils, and calibrated with the silicon photodiode. The detector was operated with fine threshold adjustment. The exposure time was set to 30 ms, corresponding to a full counting range (15 bit) at 1 MHz average count rate. The maximum detection rate obtained was 0.7 MHz. Fig. 5 shows the linearity response of some individual pixels rescaled in equivalent counts per second. One pixel has anomalously high response, probably due to double counting. All other pixels have a reduced slope above 400 kHz pixel rate, although some departure from linearity can be seen at lower input rates. The departure from linear behavior can be reproduced by a model taking into account the time structure of the beam as well as the pile-up of detected events. At the time of the tests the ESRF ring was operated in the $2 \times \frac{1}{3}$ filling mode, consisting of an active

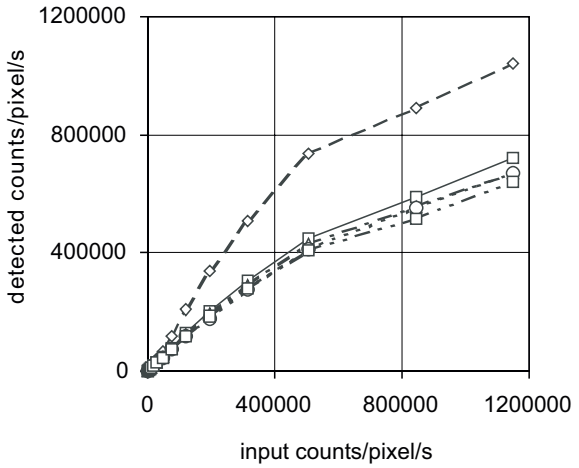

Fig. 5. Response of individual pixels as a function of input rate. The input photon rate is calculated from the beam intensity measured with a silicon photodiode and from the absorption characteristics of the silicon sensor.

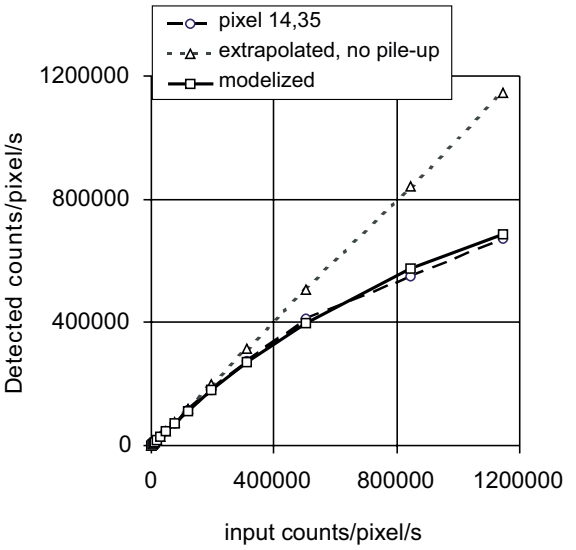

Fig. 6. Modelization of the pixel response using the analytical model of Ref. [11].

period of duration $T_a = 0.93\,\mu s$ evenly filled with about 330 electron packets or bunches of typically 40–100 ps duration, followed by an empty interval of 0.47 μs, this sequence being repeated twice during the ring period $T_r = 2.8\,\mu s$. In our model, we assume that the detector cannot discriminate multiple events within one bunch, so any number of events detected during one bunch is seen as one single event. We also assume that the effective detector recovery time in the absence of incoming hits is shorter than the inactive ring period of 0.47 μs. Finally, we assume that X-ray emission during one active period follows Poisson statistics. We are thus in a situation as depicted in Refs. [10,11] which give the details of the model calculation. The model prediction agrees well with data (Fig. 6). In particular, this confirms that: (a) in practice the detector does not discriminate more than one event per bunch, and (b) the detector recovery in the absence of hitting events is shorter than 0.47 μs. These results are consistent with a measured 2 MHz maximum counting rate under regular pulsing [1,3] and a theoretical 0.150 μs peaking time [2,9]

The pixel response non-linearity is assumed reproducible, hence correctable using an appropriate calibration procedure. However, since the detector behavior depends on the beam time structure, one calibration is necessary for each machine mode.

4.4. PSF, dynamic range

The point spread function (PSF) was measured with a pencil beam of $10 \times 10\,\mu m^2$ hitting the center of one pixel. In order to obtain a high dynamic range, we accumulated 20 exposures of 5 s each. After masking the 13 noisy pixels, the resulting PSF is shown in Fig. 7. In the central pixel 2.5×10^5 counts were collected, whereas its direct neighbors collected 5×10^3 counts (2%). Some non-symmetric wings are visible, probably caused by scattering from the collimators or from air. The background at a large distance from the illuminated pixel is of the level of 10 counts and is due to a well-known design flaw in our detector, namely that opening and closing the shutter has a chance of causing 1 count in a given pixel. Some pixels do not suffer from this effect and others show it always. This effect at present limits our dynamic range.

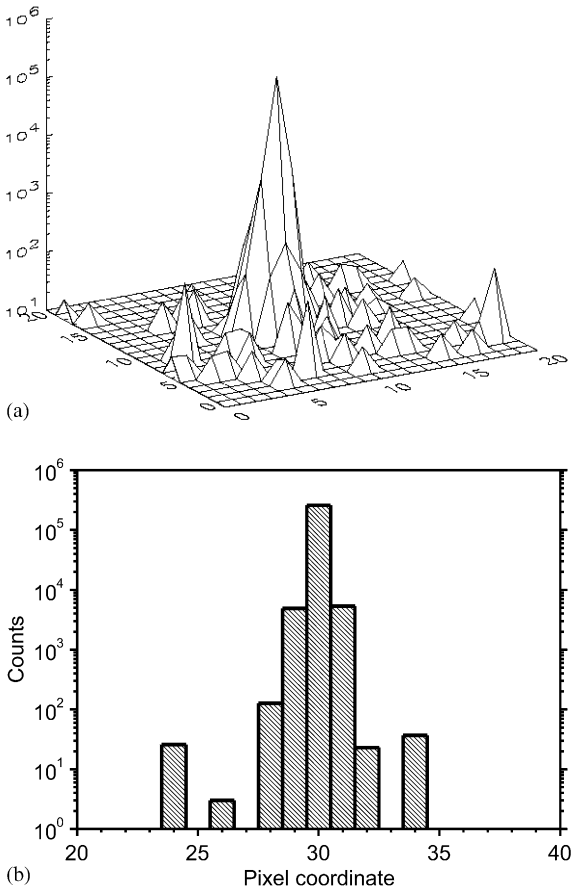

Fig. 7. (a) Point spread function resulting from 20 accumulated frames, each 1-s long. (b) Horizontal slice across the PSF of Fig. 7a. The low-intensity side lobes are interpreted as small angle air scattering.

4.5. Subpixel sensitivity scanning

An area covering a few pixels is probed in 10 μm steps in both lateral and vertical directions with a $10 \times 10\,\mu m^2$ collimated beam, one frame being acquired at each position. This test aims at investigating possible local inhomogeneities in the detection efficiency due to charge sharing between pixels in the silicon detection sensor or to other causes such as semiconductor material or bump-bonding defects. The explored region covers an area of $510 \times 160\,\mu m$. One can then reconstruct with a 10 μm precision, the sensitivity map of one particular pixel (Fig. 8) as well as of the entire explored region by combining individual pixel contributions (Fig. 9a and b). The responses of adjacent pixels cross at 50% of the counts at pixel centers (Fig. 9c), as a result the sensitivity map is particularly flat with neither loss nor doubling of counts between pixels and only a shallow drop of about 15% at the crossing point between 4 pixels. This demonstrates that the performed sensor calibration and, in particular, the threshold tuning allows to properly balance the count errors that would arise from charge sharing between two pixels. This confirms our previous finding of practically no charge loss due to charge sharing between adjacent pixels in a GaAs-based Medipix-1 imaging system, obtained with 60-keV collimated irradiation [12] as well as results obtained with other photon-counting pixel detectors [13]. Therefore, charge sharing might no longer be regarded as a major matter of concern for imaging with photon-counting pixel detectors. However, the sensitivity maps of Fig. 9 also involve some contribution from unavoidable X-rays scattered at small angle from the beam axis, and therefore are not a pure representation of the charge sharing range only. Similar tests performed on a single photon counting chip with same silicon thickness [13] report a steeper decrease of pixel response at a distance from pixel edge, probably because of a lesser amount of this small-angle scattering. In our case, the X-ray counts detected at more than 1 pixel distance from the beam center (Fig. 9d) confirm the non-negligible X-ray scatter residue.

4.6. Test image with a bar pattern

Fig. 10 shows the image of a lead bar pattern (Huttner type 1–83, 50 μm Pb). The line spatial frequency is 1.8 lp/mm, i.e. 30% of the pixel sampling frequency. The measured contrast modulation is 80%. The pixellated bar edges are characteristic of scatter-free detectors whose resolution is only limited by the pixel aperture.

4.7. Time resolution

The beam intensity is modulated using a 10 Hz rotating chopper with tungsten blades. The beam energy is 13 keV. An external signal triggers an

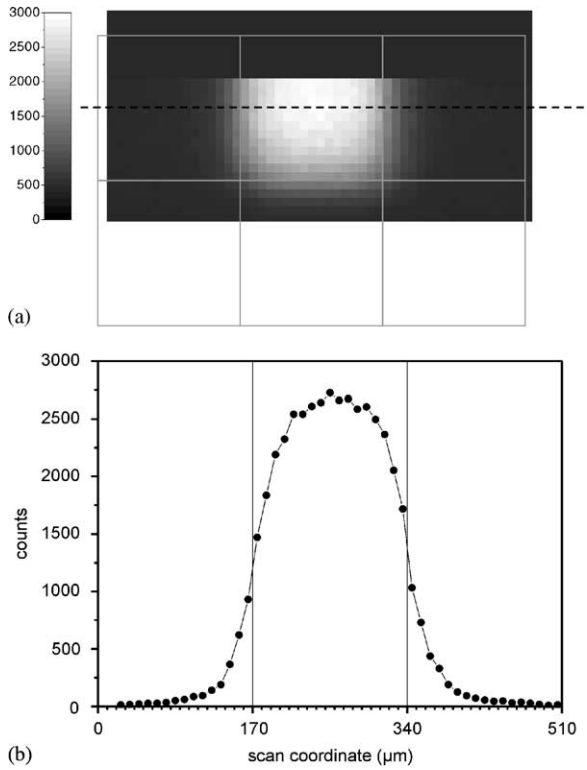

Fig. 8. Sensitivity of one pixel, mapped with 10 μm resolution. (a) Linear gray scale representation showing the insensitive (black) and counting (white) regions. The 3×2 squares overlay represents the actual location and size of a 6 pixels array at the detector surface. (b) Integrated counts profile along dotted line of Fig. 8a.

acquisition cycle every 10 ms. Each cycle consists of 3 ms count integration, 1 ms detector readout (8 Mbytes/s chip readout rate), and data transfer time to the computer, thereby achieving 100 Hz frame rate acquisition with 30% live time. A sequence of 500 frames is acquired, a subset of which covering 0.1 s acquisition time (10 frames), is shown in Fig. 11a. Each illuminated pixel collects about 300 counts, giving sufficient statistics to clearly visualize the beam occultation by the chopper blade. The corresponding absorbed flux rate is 10^5 counts/pixel/s. As a major advantage of photon counting detection, the pixel signal is absolutely free from any time lag (Fig. 11b).

4.8. Radiation damage

Submitting the detector to a strong input flux resulted in a noise increase in the irradiated area, which was interpreted as damage induced on the readout chip by transmitted X-rays through the silicon sensor. The damage is deemed permanent since no partial recovery was observed after a few hours. We roughly estimate the corresponding cumulated dose as follows: with the monitoring photodiode (0.54 μA photocurrent, diode in beam, 40% transmission at 13 keV, $1.5 \times 1.5\,\mathrm{mm}^2$) we estimate the photon flux to be 2.7×10^8 photons/mm^2/s on the silicon sensor i.e. 1.1×10^8 photons/mm^2/s reaching the readout chip (40% silicon sensor transmission). The dose equivalent in silicon is 3 Gy/10^9 photon/mm^2 at 13 keV (Silicon density = 2.33 g/cm^3 and $\mu_{\mathrm{Si}} = 3.42\,\mathrm{mm}^{-1}$). This means in our case: 0.8 Gy/s on the silicon sensor and 0.32 Gy/s reaching the readout chip surface. For an estimated cumulated exposure time of about 2 min, this leads to an absorbed dose of 10 krad (or 100 Gy or 3×10^{10} photon/mm^2) in the

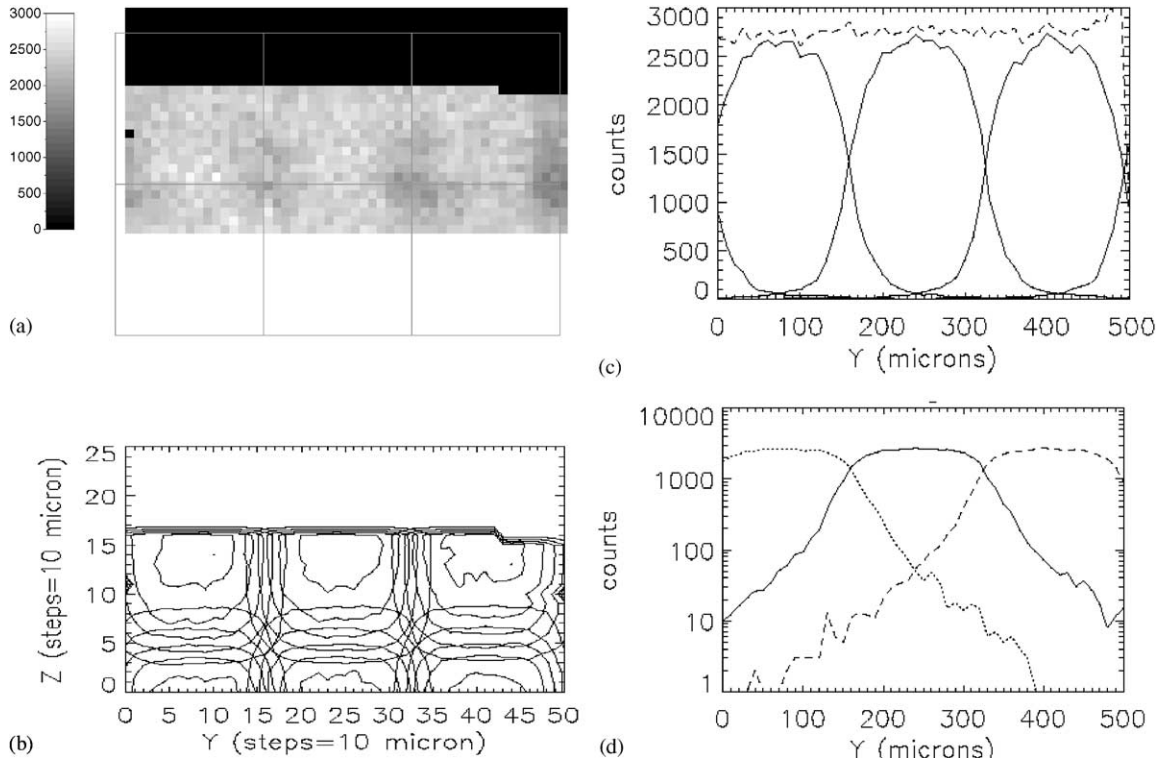

Fig. 9. Local detector sensitivity after summing the contributions of adjacent pixels: (a) image representing the total number of detected counts at a given position of the scanning beam. The slightly lower response areas are located at the crosspoint of 4 pixels; (b) contour plot representation, each closed line connects points of equal sensitivity; (c) horizontal slice across pixel centers; (d) same as (c), log scale.

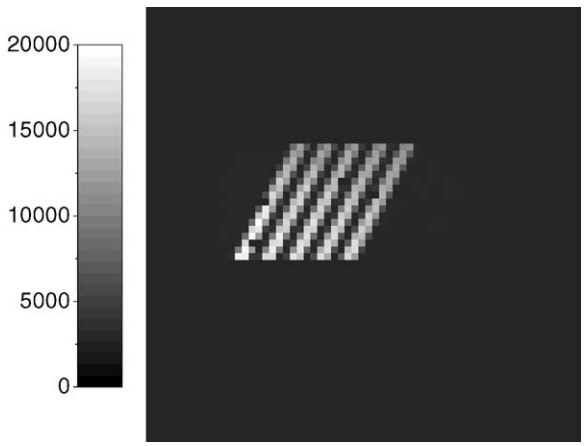

Fig. 10. Image of a lead bar pattern of 1.8 lp/mm spatial frequency.

silicon sensor, and of 4 krad (or 40 Gy or 1.3×10^{10} photon/mm^2) in the readout chip. These numbers must be regarded as orders of magnitude.

Considerations for use at a synchrotron source: for strong diffraction spots obtained at an undulator or wiggler source, with typical intensities of 10^5 photons/s i.e. 10^6 photons/mm^2/s, we find that radiation damage at the spot location, for 13 keV photon energy, requires more than 8 h cumulated exposure. Alternatively, accidental exposure to the direct beam (10^{10}–10^{13} photons/mm^2/s) as can occur during beamstop alignment may locally damage the detector in less than a second. Therefore, a higher radiation hardness is suitable considering regular use of the detector on a synchrotron source. In this respect, major improvements are expected from the next Medipix

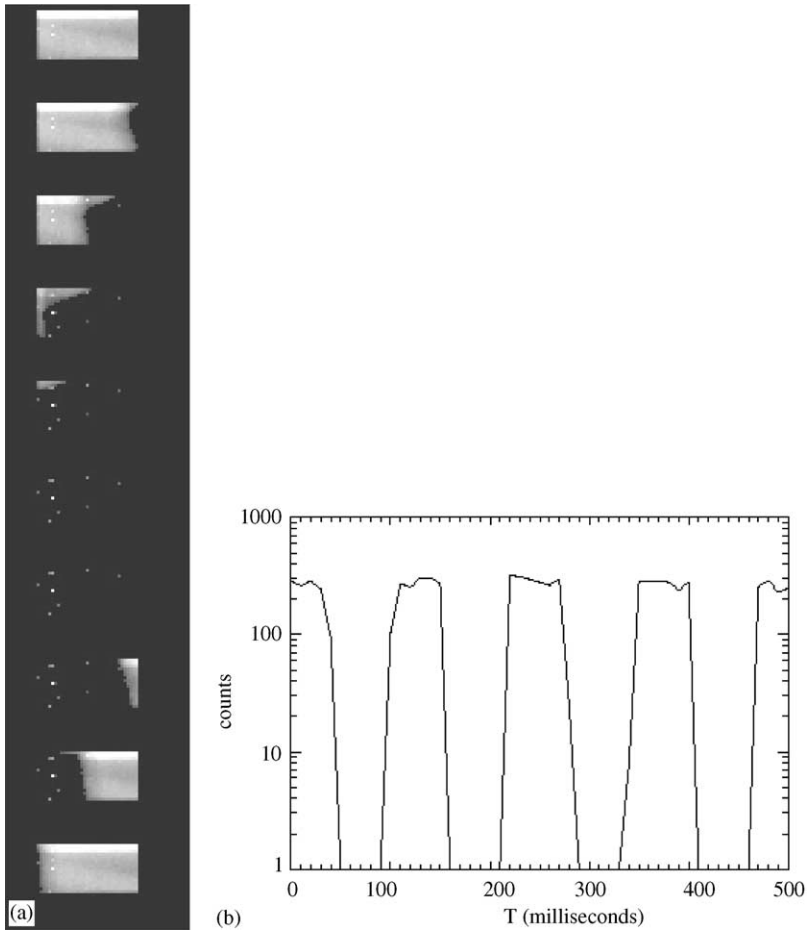

Fig. 11. Dynamic acquisition at 100 Hz frame rate of a beam modulated with a 10 Hz chopper: (a) sequence of 10 images, covering 0.1 s duration; (b) response of a particular pixel during the same acquisition sequence.

chip version based on deep-sub micron CMOS technology, as well as from the use of thicker or more absorbing detector sensors.

5. Conclusions

We have demonstrated the following features of a photon counting Medipix-1 imaging system illuminated by a synchrotron beam: an energy response down to 6 keV after individual threshold tuning, a time resolution up to 100 Hz frame rate, a pixel-limited point-spread function, and a seamless sensitivity with no signal loss at pixel edges. This latter point shows that for a given X-ray energy, charge sharing between neighboring pixels can be compensated by proper threshold calibration, thereby eliminating its detrimental consequence on imaging performance. The main issues with regard to possible use of the Medipix-1 detector under intense photon flux are at present the radiation damage threshold, and the non-linear behavior at high event rate: the first point is inherent to the readout chip technology and will be greatly alleviated in the next CMOS-based chip versions. The second point, related to photon counting detection, may be managed by proper pixel response calibration, taking into account the

time structure of the beam. Finally, the present evaluation confirms the usability of counting pixel detectors as X-ray imaging devices for synchrotron applications, and also motivates for further evaluations involving the pulsed beam time structure and the photon counting corrections at high event rate.

Acknowledgements

The Medipix-1 circuit was developed as part of the Medipix project carried out originally by CERN (Geneva, Switzerland), University of Freiburg (Germany), University of Glasgow (UK), and INFN and the Universities of Pisa and Napoli, (Italy). We would like to warmly thank all the staff of the BM5 ESRF beamline for their assistance during the tests.

References

[1] M. Campbell, et al., Readout for a 64×64 pixel matrix with 15-bit single photon counting, IEEE Trans. Nucl. Sci. 45 (1998) 751.

[2] B. Mikulec, Single photon detection with semicondutor pixel arrays for medical applications, Ph.D. Thesis, University of Vienna, Austria, 2000.

[3] M.G. Bisogni, et al., Performance of a 4096 pixel photon counting chip, Proc. SPIE 3445 (1998) 31.

[4] A. Fornaini, et al., Soft X-ray sensitivity of a photon-counting hybrid pixel detector with a silicon sensor matrix, Nucl. Instr. and Meth. A 466 (2000) 142.

[5] S.R. Amendolia, et al., Low contrast imaging with a GaAs pixel digital detector, IEEE Trans. Nucl. Sci. 47 (2000) 1478.

[6] S.R. Amendolia, et al., Test of a GaAs-based pixel device for digital mammography, Nucl. Instr. and Meth. A 460 (2001) 50.

[7] E. Heijne, LHC1: A semiconductor pixel detector readout chip with internal, tunable delay providing a binary pattern of selected events, Nucl. Instr. and Meth. A 383 (1996) 55.

[8] G. Bardelloni, et al., A new read-out system for an imaging pixel detector, Proceedings of the IEEE Nuclear Science Symposium and Medical Imaging Conference, Lyon, France, 2000, Sect. 12, pp. 57–60.

[9] B. Mikulec, et al., Characterization of a single photon counting pixel system for imaging of low-contrast objects, Nucl. Instr. and Meth. A 458 (2001) 352.

[10] C. Ponchut, Pixel detectors in counting mode: limitations induced by the pulsed time structure of the X-ray beam, ESRF Internal note CP/16/99, 1999.

[11] J.E. Bateman, The effect of beam time structure on counting detectors in SRS experiments, J. Synchr. Radiat. 7 (2000) 307.

[12] L. Abate, et al., Noise and interpixel dead space studies of GaAs pixellated detectors, Nucl. Instr. and Meth. A 458 (2001) 164.

[13] C. Broennimann, et al., Synchrotron beam test with a photon-counting X-ray detector, J. Synchr. Radiat. 7 (2000) 301.